Triggering of flow asymmetry by anisotropic deflection of lamella during the impact of a drop onto superhydrophobic surfaces

Kartik Regulagadda, Shamit Bakshi, and Sarit Kumar Das

Articles you may be interested in

Morphology of drop impact on a superhydrophobic surface with macro-structures
Physics of Fluids **29**, 082104 (2017); 10.1063/1.4997266

Ionic solubility and solutal advection governed augmented evaporation kinetics of salt solution pendant droplets
Physics of Fluids **30**, 012113 (2018); 10.1063/1.5013356

Referee Acknowledgment for 2017
Physics of Fluids **30**, 010201 (2018); 10.1063/1.5022671

Dynamics of a flexible superhydrophobic surface during a drop impact
Physics of Fluids **30**, 072102 (2018); 10.1063/1.5028127

Publisher's Note: "Effect of grid resolution on large eddy simulation of wall-bounded turbulence" [Phys. Fluids 30, 055106 (2018)]
Physics of Fluids **30**, 079901 (2018); 10.1063/1.5048433

Numerical study of laminar boundary-layer flows over a superhydrophobic plate
Physics of Fluids **30**, 072002 (2018); 10.1063/1.5039605

Triggering of flow asymmetry by anisotropic deflection of lamella during the impact of a drop onto superhydrophobic surfaces

Kartik Regulagadda, Shamit Bakshi,[a)] and Sarit Kumar Das[b)]
Department of Mechanical Engineering, Indian Institute of Technology, Madras, Tamil Nadu 600036, India

A water drop impacting a superhydrophobic surface (SHS) rebounds completely with remarkable elasticity. For a given drop size, the time of contact on a flat SHS remains constant. However, recent studies show that the contact time can be reduced further by triggering an asymmetry in the hydrodynamics of impact. This can be achieved in different ways; an example being the impact on a cylindrical SHS with a curvature comparable to the drop. Here, the anisotropic flow generated from the tangential momentum and elliptical footprint of the drop before the crash leads to the formation of lobes. In the present work, we perform drop impact experiments on a bathtub-like SHS and show that the radial anisotropy can be triggered even in the absence of both the tangential momentum and noncircular footprint. This is shown to be a consequence of lamella deflection during the drop spreading. The reduction in contact time is quite clearly evident in this experimental regime. *Published by AIP Publishing.* https://doi.org/10.1063/1.5041824

I. INTRODUCTION

The impact of a droplet onto solid surfaces is ubiquitous in nature and practical applications. The patterns of the impact as discussed in the pioneering work of Worthington[1] brought out a significant understanding of the hydrodynamics. Various studies over the years revealed that surface wettability is a key factor in deciding the outcome of impact. The first investigation of Wenzel[2] in designing water-repellent fabrics made significant progress in analysing the surface wettability. This analysis is extended to porous surfaces by Cassie and Baxter.[3] Later, it was shown that the manipulation of surface texture can produce superhydrophobic surfaces (SHSs) with remarkable water-repellency.[4]

In this context, it may be useful to look at the example of the spray cooling process. This is a technique where cold drops are impinged onto hot surfaces to remove heat. However, when the surface temperature is at/above the Leidenfrost point, a complete drop rebound is observed. This is due to the formation of a stable vapour film between the impacting drop and the surface.[5,6] The vapor film reduces the time of drop-surface interaction and drastically reduces the effectiveness of the spray cooling process. On the contrary, some applications like anti-icing,[7,8] self-cleaning,[9–11] and so on require rapid shedding of the drop. This can be achieved with low energy surfaces like SHSs (without heating the surface). Richard *et al.*[12] showed that the contact time of a bouncing drop on a macroscopically flat SHS is constant for a wide range of Weber numbers ($We > 1$), where $We = \rho U_0^2 R_0/\sigma$ (ρ is the density of the liquid, U_0 is the impact velocity of the drop, R_0 is the radius of the drop before impact, and σ is the surface tension of the liquid). The time of contact on a SHS scales linearly with the inertio-capillary time scale $\tau = \sqrt{\rho R_0^3/\sigma}$. The contact time in the above-mentioned *We* regime is found to be around 2.6τ, which is a theoretical limit (minima) that can be achieved on any flat surface. During the impact, the drop forms a pancake-like structure at the point of maximum spread and recoils to lift-off maintaining a radial symmetry.

In freezing rain, ice accretion on surfaces can occur if the time scale of ice nucleation is comparable to the contact time of the drop. Despite exhibiting a complete drop rebound, the SHS still suffers from ice formation under adverse environmental conditions.[13–15] Thus the constant contact time on a flat SHS is a serious limitation. However, recent studies[16–18] have shown that the contact time can be reduced (below 2.6τ) by breaking the radial symmetry of impact. Bird *et al.*[16] achieved this anisotropy in an impacting drop by introducing macroscopic ridges on a flat SHS. Liu *et al.*[17] brought about the anisotropy by impacting drops onto a cylindrical SHS with a curvature comparable to the drop. The main reasons for flow anisotropy leading to rapid bouncing were identified as the elliptical footprint and tangential (parallel to the surface) momentum of the drop prior to the impact.[17] Recently, Regulagadda *et al.*[19] showed that the post-impact morphology of the anisotropic flow could be very different based on the impact configurations.

The mere presence of the tangential momentum prior to impact may not necessarily reduce the contact time (as in the case of impacts onto a spherical SHS).[17,20] However, a spatially non-uniform distribution of the tangential momentum can potentially reduce it, as shown in Fig. 1. During an oblique impact on a flat SHS, modest or no reduction in contact time can be observed as the tangential momentum is uniform around the axis of the drop.[21] For impacts onto cylinders, the drop has a spatial gradient in the tangential momentum, resulting in a contact time reduction.[17,22] Furthermore, the footprint of the drop during the crash is non-circular. Yun[23] had experimentally shown that the contact time of an ellipsoidal drop on a

a)Electronic mail: shamit@iitm.ac.in
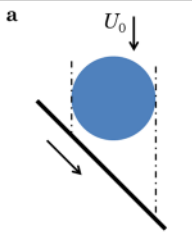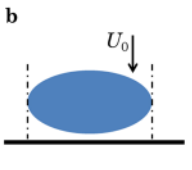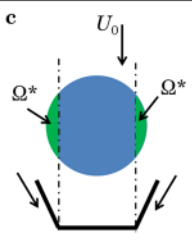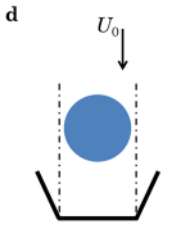b)Present address: Department of Mechanical Engineering, Indian Institute of Technology, Ropar 140001, India.

Sketch	M_t - Tangential momentum of the impacting drop	Volume on which M_t acts	SHS type	Footprint	Contact time reduction
a	✓	Complete drop volume	Flat	Circular	Modest / No
b	✗	None	Flat	Elliptical	Yes
c	✓	Only on the spherical segments (Ω^*)	Bathtub	Non-circular	Yes
d	✗	None	Bathtub	Circular	Addressed in this paper

FIG. 1. Sketch showing different impact configurations: (a) oblique impact of a spherical drop on a flat SHS, (b) normal impact of an ellipsoidal drop on a flat SHS, and (c) and (d) normal impact of a spherical drop on a bathtub-like SHS.

flat SHS can be 30% lower than that of a spherical drop with equal volume. The above studies demonstrate that the non-uniform tangential momentum and/or non-circular footprint of the impacting drop trigger the anisotropic flow, leading to the reduction in the contact time.

In the present work, we have designed our experiments in a way that the drop footprint can be changed from non-circular to circular. Consequently, the non-uniform tangential momentum of the impacting drop (from here on, this is simply referred to as tangential momentum) changes from non-zero to zero [see Figs. 1(c) and 1(d)]. From these experiments, we can observe an intermediate regime where the radially anisotropic flow is triggered even in the absence of any tangential momentum or non-circular footprint. The detailed description of the experimental setup and procedure is given in Sec. II.

II. EXPERIMENTAL METHOD

Figure 2 shows the setup (not to scale) used for the drop impact experiments. Isosceles trapezoidal cross sections (bathtub-like) are machined on substrates (see Fig. 3) using

the wire-cut electric discharge machining process with varying flat base width ($0 \leqslant w \leqslant 8$ mm). For $0 < w < D_0$ (D_0 is the drop diameter), it should be noted that the drop impinges partly onto the inclined face during the crash [see Figs. 3(a)
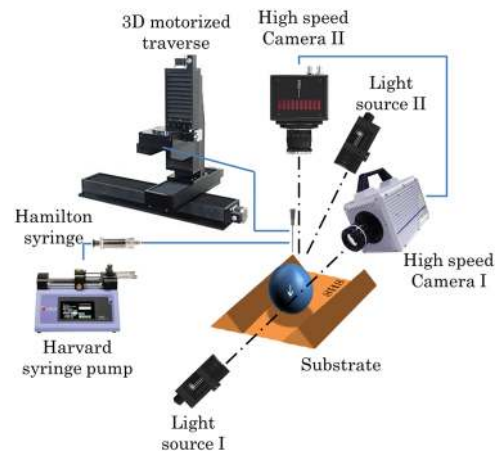

FIG. 2. The setup used in the experiments. The image shown is not to scale.
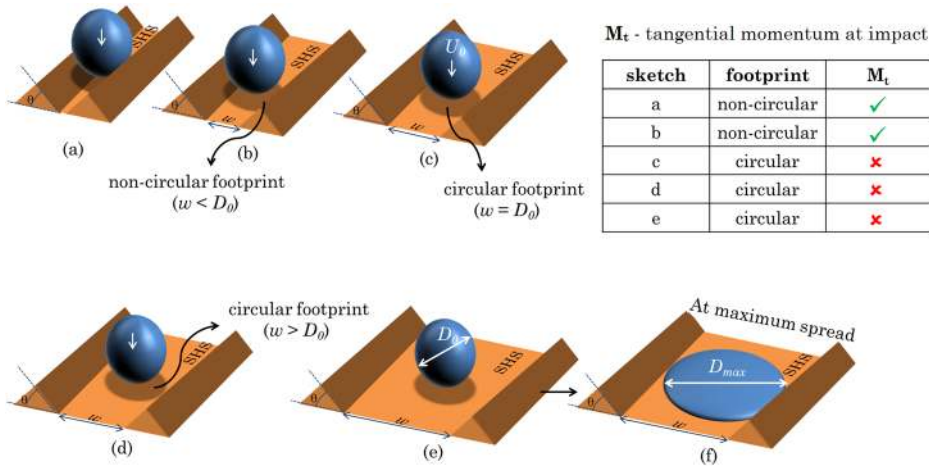
FIG. 3. Sketch showing the configuration of impact. Sketches (a) and (b) indicate the configuration where $w < D_0$. It can be clearly seen that the footprint or the shadow of the drop on the substrate intersects with the inclined faces. Thus, the footprint is non-circular along with the presence of the tangential momentum. However, sketches from (c) to (f) show the configurations where both the features are absent ($w \geqslant D_0$). Sketch f indicates the maximum w considered in the experiments so that the liquid lamella never climbs the inclined face at $We \sim 21$.

and 3(b)]. Furthermore, the footprint is non-circular. To eliminate these two effects on the impact hydrodynamics, the width of the flat region (w) is increased in steps. Thus, $w \geqslant D_0$ indicates the configuration having zero tangential momentum with a circular footprint [see Figs. 3(c)–3(f)]. The maximum value of w is selected in a way that the droplet after the end of spreading remains completely within the flat valley at $We \sim 21$ [see Fig. 3(f)]. The angle (θ) of the trapezoidal sections is selected to be 5°, 15°, 25°, 45°, and 60°. All the substrates are coated with superhydrophobic coatings from Ultra Ever Dry, Inc. The contact angle (>160°) and the roll-off angle (<5°) for the flat substrate indicate the superhydrophobic behavior.[24] Water droplets (HPLC grade) are impacted onto the center of the flat base with $We \sim 10$, 21, and 28 from a calibrated needle with an outer diameter of 0.72 mm. The needle is positioned approximately at the flat base center with the aid of a 3D motorized traverse. The radius of the droplet in the experiments is $R_0 = 1.49 \pm 0.02$ mm, unless otherwise stated. The density and surface tension values of water are taken as 1000 kg/m^3 and 0.073 N/m, respectively. The impacts are recorded using synchronised high-speed cameras (Photron SA4 and Fastcam

Mini UX100) from the side and top views with a frame rate of 8000 Hz. All the images are processed using open source image software Fiji ImageJ (1.51n). The contact time is the interval between the first time instant when any point of the drop surface comes in contact with the solid substrate and the time instant of complete liquid detachment from the substrate. This is obtained from the side view images. The configuration of an impact is represented as S_{w/D_0}^{θ}. Thus, $S_{0.17}^{45°}$ represents the impact with $\theta = 45°$ and $w/D_0 = 0.17$.

III. CONTACT TIME

Figure 4 (Multimedia view) shows the drop impact morphology of $S_{0.17}^{45°}$ and $S_1^{45°}$ configurations at $We \sim 21$. In $S_{0.17}^{45°}$ ($w < D_0$), the footprint of the drop is non-circular and tangential momentum is present. Hence, the flow asymmetry and the resultant reduction in the contact time can be attributed to these factors.[17,19] A jet along the valley can be noticed in the top view images of Fig. 4(a) (Multimedia view). The stretch of the jet is dependent on the magnitude of the tangential momentum imparted to the drop. As w decreases, the volume of the

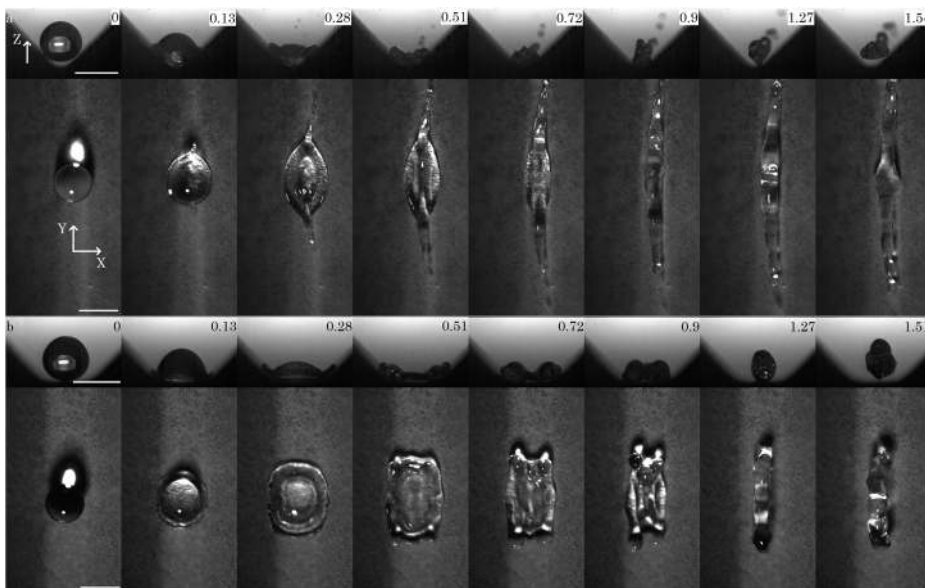FIG. 4. Side and top views of impact configuration: (a) $S_{0.17}^{45°}$, $We = 19.8$ and (b) $S_1^{45°}$, $We = 22.2$. The time indicated in each frame is non-dimensionalized with the inertio-capillary time scale (τ). The scale bars in the insets represent 3 mm. The videos are available in the supplementary material. Multimedia views: https://doi.org/10.1063/1.5041824.1; https://doi.org/10.1063/1.5041824.2

spherical segment (of the drop) interacting with the inclined face increases, producing a higher tangential momentum and a longer stretch of the jet.[19] We can also observe the formation of secondary droplets from the jet. Interestingly, the configurations with $w \geqslant D_0$ [see Fig. 4(b) (Multimedia view)] produce asymmetric structures even though the tangential momentum, as well as the non-circular footprint, is absent. The recoiling of the drop is rapid downhill, allowing early lift-off in comparison with a flat SHS. Experiments were performed on the substrates with different angles (θ). Similar results were noticed for $S^{15°}$, $S^{25°}$, and $S^{60°}$ (see the supplementary material for movies).

Figure 5 shows the contact time plotted against w/D_0 for all the impact configurations (S_{w/D_0}^{θ}) at $We \sim 21$. For the regime where the tangential momentum exists ($w < D_0$), the contact time reduction is substantial and fairly constant for a fixed θ. It should be noted that the reduction in the case of $S^{5°}$ is not appreciable as this configuration is close to a flat surface. In the $w \geqslant D_0$ regime, the contact time rapidly increases with w. Here, the asymmetry is triggered by the deflection of a part of lamella as other mechanisms are absent. As w approaches D_{max} (maximum spread), the contact time is same as that of a flat SHS as no lamella deflection takes place. Similar results are observed at $We \sim 10$ and 28 (see the supplementary material). Additional experiments are performed to study the effect of impact velocity on the phenomenon by varying the drop release height. It can be observed from Fig. 6(a) that the contact time reduces as We is increased (for a fixed w). We also performed experiments with a drop diameter (D_0) of ~ 1.8 mm at $We \sim 11$. Once again, we can observe the contact time reduction in the $w \geqslant D_0$ regime [see Fig. 6(b)]. Finally, the effect of inclination angle θ on the contact time in this regime can be noticed in Fig. 5. As θ decreases, the rate at which the contact time (τ_s/τ) approaches the value 2.6 (contact time on a flat SHS) increases. Thus, the contact time reduction because of the lamella deflection is evident over a wide range of Weber numbers, droplet diameters, and configurations of the macro-structure.

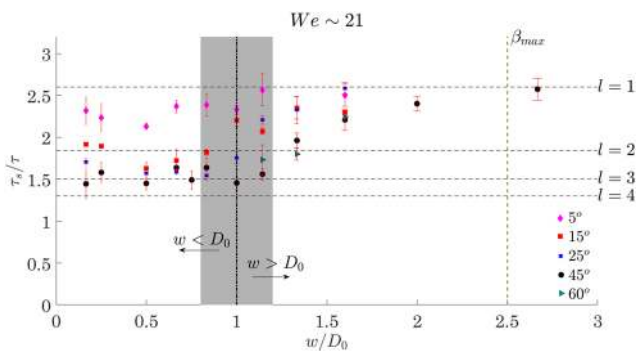Figures 5 and 6(b) also show the contact time calculated from the number of lobes (l), as defined by Gauthier *et al.*[25] The

FIG. 6. (a) Figure showing the variation of non-dimensional contact time (τ_s/τ) with We for different w/D_0 (of $S^{45°}$) and a drop diameter of $D_0 \sim 2.98$ mm. As We increases, the contact time reduction is higher except for $w/D_0 = 2.7$ which acts as a flat surface for the selected We. (b) Plot showing the variation of non-dimensional contact time (τ_s/τ) with w/D_0 for a drop diameter of $D_0 \sim 1.8$ mm at $We \sim 11$. The contact time reduction in the $w \geqslant D_0$ regime is evident here also. The error bars in both the plots indicate the uncertainty in the contact time.

flow anisotropy leads to the redistribution of the droplet volume (V_0) into lobes which have lower volume ($V_l < V_0$). The reduced inertio-capillary time for a lobe is given by $\sqrt{\rho V_l^3/\sigma}$ ($V_l = V_0/l$). This approach holds good only when the droplet volume is distributed equally in all the lobes. However, in the present experiments, the droplet volume is not equally distributed in the lobes. Thus, we can notice that (in Figs. 5 and 6) the contact time falls in the window of non-integer values of l (between 1-2, 2-3, and so on). This is similar to the impacts at an offset to a ridge as mentioned in the supplementary material of Gauthier *et al.*[25]

To investigate the spreading dynamics of the impact in the $w \geqslant D_0$ regime, we consider the spread in two directions, namely, X and Y [see Fig. 4 (Multimedia view) and the insets of Fig. 7(a)]. The spread length along X (obtained from the side view) is the projection of the actual spread on the surface as a portion of the drop spreads on the inclined face. Hence, we consider the total spread length (D_{total}) parallel to the surface at any time t [see the inset of Fig. 7(a)]. It should be noted that D_{total} is the summation of the spread lengths on the flat and inclined regions. If D_x represents the horizontal spread length [as shown in the inset of Fig. 7(a)] at any time instant t, then

$$D_{total} = \left\{ \begin{matrix} w + (D_x - w)/\cos\theta & \forall & D_x > w \\ \\ D_x & \forall & D_x \leqslant w \end{matrix} \right\}.$$

The spread length along the valley (obtained from the top view) at the same time instant t is considered to be D_y.

FIG. 5. Plot showing the non-dimensional contact time (τ_s/τ) with w/D_0 at $We \sim 21$ for a drop diameter of $D_0 \sim 2.98$ mm. Here, β_{max} indicates the maximum spread length non-dimensionalised with the drop diameter D_0 on a flat substrate for $We \sim 21$. The number of lobes formed during impact on macro-ridges as defined by Gauthier *et al.*[25] is indicated by l. The dashed horizontal line acts as a guide to the eye. The error bars show the uncertainty in the contact time.
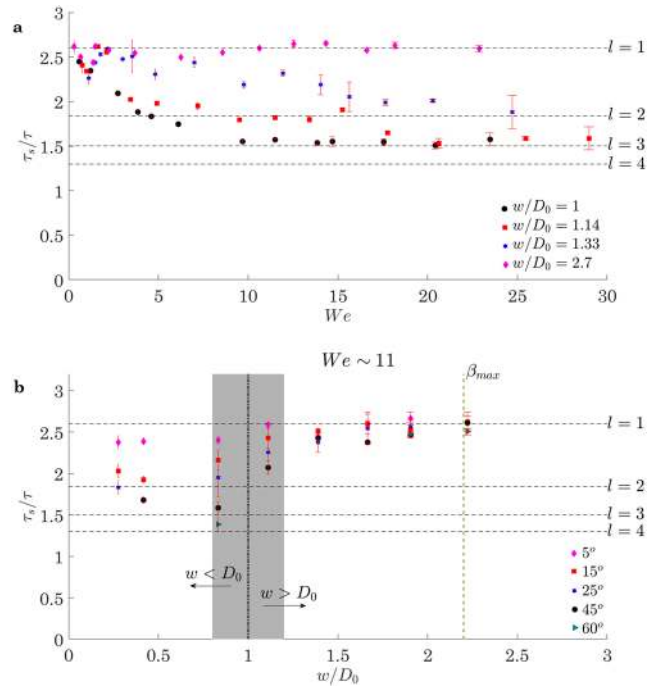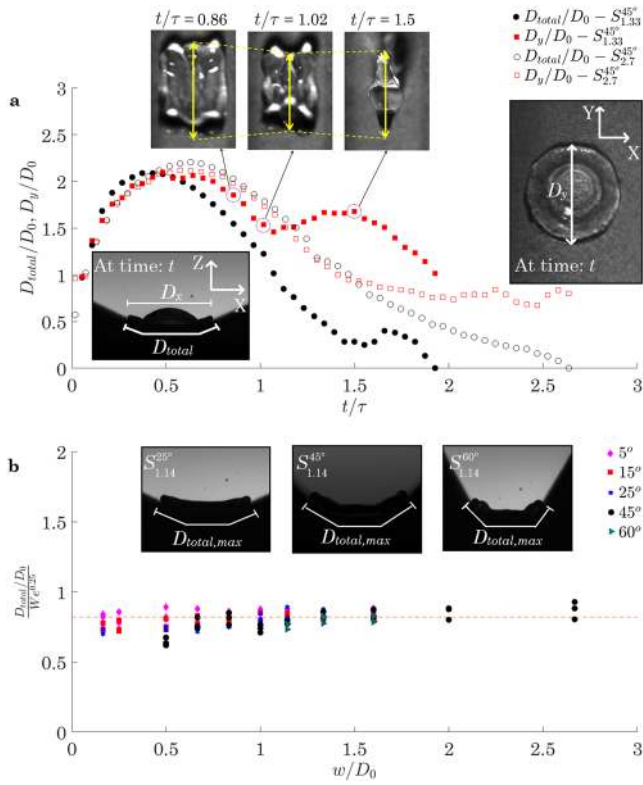
FIG. 7. (a) Plot showing the non-dimensional spread length (D_{total}/D_0 and D_y/D_0) with time (t/τ) of $S_{1.33}^{45°}$ and $S_{2.7}^{45°}$ configurations at $We \sim 21$ for a drop diameter of $D_0 \sim 2.98$ mm. The images in the inset show D_{total}, D_x, and D_y at any time instant t. Additional snapshots in the inset indicate the variation of D_y with t/τ at selected time instants. The local minimum of D_y can be clearly observed during the recoiling phase. (b) Plot showing $\frac{D_{total,max}/D_0}{We^{0.25}}$ with w/D_0 for $We \sim 10$, 21, and 28. The value of $D_{total,max}/D_0$ matches well with the scaling of Clanet *et al.*[26] and remains fairly constant for all the configurations in the regime $w \geqslant D_0$. Images in the inset show the $D_{total,max}$ for $S_{1.14}$ configurations at $We \sim 21$. The dashed horizontal line indicates the average of $D_{total,max}$ in the $w \geqslant D_0$ regime.

In the Y-direction, the liquid always stays in the flat region and hence the measurement is similar to the $D_x < w$ case. We consider the configurations $S_{1.33}^{45°}$ and $S_{2.7}^{45°}$ at $We \sim 21$ to show the time evolution of D_{total} and D_y [see Fig. 7(a)]. The plot shows that $D_{total} \sim D_y$ up to the time to reach maximum D_{total} in both the configurations. In fact, $D_{total,max}/D_0 \sim We^{0.25}$ matches well with the scaling of Clanet *et al.*[26] for all the $S_{w \geqslant D_0}^{\theta}$ configurations [see Fig. 7(b)]. This signifies that the spread length is fairly isotropic even in the presence of the inclined face in the X direction during the inertial regime. This could be due to the fact that the spreading is more dependent on the rim inertia which should be similar (during most of the spreading phase) in both the cases. The anisotropy in the lamella gets triggered only toward the end of the spreading or the beginning of the retraction phase. Thus the recoiling in the X-direction is rapid compared to the Y-direction, as shown in Fig. 7(a) (for $S_{1.33}^{45°}$). The velocity of retraction in the Y-direction is fairly comparable to that of a flat SHS during the initial stages of recoiling. It should be noted that there is a local minimum of D_y in $S_{1.33}^{45°}$ configuration (see the snapshots in the inset of Fig. 7). This is because of the globule formation, as shown in the inset of Fig. 7(a). The globules are formed due to the internal flow structure developed within the droplet. D_y keeps

on reducing until a point in time where the globules formed on either side of Y-axis (valley) merge. This fusion of globules increases D_y temporarily, as shown in the snapshots (inset) of Fig. 7(a). Finally, the drop lifts-off before the recoiling in the Y-direction is complete.

IV. CONCLUSION

With a systematic experimental procedure, we have shown that the non-uniform tangential component of the momentum and non-circular footprint of an impacting drop onto SHS is not always a requirement to produce anisotropic flows during a drop impact. Even a lamella deflection can trigger the flow asymmetry and eventually reduce the contact time. This is demonstrated with the aid of the bathtub geometry of SHS. The phenomenon is dependent on the ratio of flat region width (of the bathtub) to drop diameter (w/D_0), inclination of the sloping face of the bathtub (θ), and the Weber number (We). The effect of each parameter on the contact time is studied in the $w > D_0$ regime (where the lamella deflection takes place). Keeping the other parameters constant in this regime, a decrease in w/D_0 results in a higher contact time reduction. Furthermore, the variation of contact time with w/D_0 is very rapid in this regime. For a given w/D_0, an increase in θ or We results in lower contact times. The spread length in the inertial regime is fairly isotropic even though the bathtub structure deflects the lamella. However, anisotropic flow is initiated internally in the lamella resulting in rapid recoil along the inclined face than along the valley. This anisotropy in recoiling leads to asymmetric liquid structures (which lift off separately), resulting in contact time reduction.

SUPPLEMENTARY MATERIAL

See supplementary material for the videos pertaining to a selected impact configurations (S_{w/D_0}^{θ}). Movie 1: Drop impact movie with configuration $S_{0.5}^{45°}$ ($We = 21.4$, $D_0 = 2.98$ mm). Movie 2: Drop impact movie with configuration $S_{1.14}^{45°}$ ($We = 20.5$, $D_0 = 2.98$ mm). Movie 3: Drop impact movie with configuration $S_{1.6}^{45°}$ ($We = 22.3$, $D_0 = 2.98$ mm). Movie 4: Drop impact movie with configuration $S_{2.7}^{45°}$ ($We = 20.7$, $D_0 = 2.98$ mm). Movie 5: Drop impact movie with configuration $S_{1.14}^{25°}$ ($We = 21.6$, $D_0 = 2.98$ mm). Movie 6: Drop impact movie with configuration $S_{1.6}^{25°}$ ($We = 22.8$, $D_0 = 2.98$ mm). Movie 7: Drop impact movie with configuration $S_{1.14}^{60°}$ ($We = 22.7$, $D_0 = 2.98$ mm). Movie 8: Drop impact movie with configuration $S_{1.6}^{60°}$ ($We = 21.4$, $D_0 = 2.98$ mm). Movie 9: Drop impact movie with configuration $S_{1.33}^{45°}$ ($We = 11.1$, $D_0 = 2.98$ mm). Movie 10: Drop impact movie with configuration $S_{1.33}^{45°}$ ($We = 26.4$, $D_0 = 2.98$ mm). Movie 11: Drop impact movie with configuration $S_{1.11}^{45°}$ ($We = 11.4$, $D_0 = 1.8$ mm).

ACKNOWLEDGMENTS

[1] A. M. Worthington, "On the forms assumed by drops of liquids falling vertically on a horizontal plate," Proc. R. Soc. London **25**, 261–272 (1876).
[2] R. N. Wenzel, "Resistance of solid surfaces to wetting by water," Ind. Eng. Chem. **28**, 988–994 (1936).

[3] A. B. D. Cassie and S. Baxter, "Wettability of porous surfaces," Trans. Faraday Soc. **40**, 546–551 (1944).

[4] T. Onda, S. Shibuichi, N. Satoh, and K. Tsujii, "Super-water-repellent fractal surfaces," Langmuir **12**, 2125–2127 (1996).

[5] S. Chandra and C. T. Avedisian, "On the collision of a droplet with a solid surface," Proc. R. Soc. A **432**, 13–41 (1991).

[6] T. Tran, H. J. J. Staat, A. Prosperetti, C. Sun, and D. Lohse, "Drop impact on superheated surfaces," Phys. Rev. Lett. **108**, 036101 (2012).

[7] L. Cao, A. K. Jones, V. K. Sikka, J. Wu, and D. Gao, "Anti-icing superhydrophobic coatings," Langmuir **25**, 12444–12448 (2009).

[8] S. Jung, M. Dorrestijn, D. Raps, A. Das, C. M. Megaridis, and D. Poulikakos, "Are superhydrophobic surfaces best for icephobicity?," Langmuir **27**, 3059–3066 (2011).

[9] W. Barthlott and C. Neinhuis, "Purity of the sacred lotus, or escape from contamination in biological surfaces," Planta **202**, 1–8 (1997); e-print arXiv:1011.1669v3.

[10] A. Marmur, "The lotus effect: Superhydrophobicity and metastability," Langmuir **20**, 3517–3519 (2004).

[11] D. Quere and M. Reyssat, "Non-adhesive lotus and other hydrophobic materials," Philos. Trans. R. Soc., A **366**, 1539–1556 (2008).

[12] D. Richard, C. Clanet, and D. Quéré, "Contact time of a bouncing drop," Nature **417**, 811 (2002).

[13] S. A. Kulinich and M. Farzaneh, "How wetting hysteresis influences ice adhesion strength on superhydrophobic surfaces," Langmuir **25**, 8854–8856 (2009).

[14] A. J. Meuler, J. D. Smith, K. K. Varanasi, J. M. Mabry, G. H. McKinley, and R. E. Cohen, "Relationships between water wettability and ice adhesion," ACS Appl. Mater. Interfaces **2**, 3100–3110 (2010).

[15] S. Jung, M. K. Tiwari, N. V. Doan, and D. Poulikakos, "Mechanism of supercooled droplet freezing on surfaces," Nat. Commun. **3**, 615 (2012).

[16] J. C. Bird, R. Dhiman, H. M. Kwon, and K. K. Varanasi, "Reducing the contact time of a bouncing drop," Nature **503**, 385–388 (2013).

[17] Y. Liu, M. Andrew, J. Li, J. M. Yeomans, and Z. Wang, "Symmetry-breaking in drop bouncing on curved surfaces," Nat. Commun. **6**, 1–8 (2015); e-print arXiv:1511.00064.

[18] P. B. Weisensee, J. Tian, N. Miljkovic, and W. P. King, "Water droplet impact on elastic superhydrophobic surfaces," Sci. Rep. **6**, 30328 (2016).

[19] K. Regulagadda, S. Bakshi, and S. K. Das, "Morphology of drop impact on a superhydrophobic surface with macro-structures," Phys. Fluids **29**, 082104 (2017).

[20] S. Chen and V. Bertola, "Drop impact on spherical soft surfaces," Phys. Fluids **29**, 082106 (2017).

[21] Y. H. Yeong, J. Burton, E. Loth, and I. S. Bayer, "Drop impact and rebound dynamics on an inclined superhydrophobic surface," Langmuir **30**, 12027–12038 (2014).

[22] X. Liu, Y. Zhao, S. Chen, S. Shen, and X. Zhao, "Numerical research on the dynamic characteristics of a droplet impacting a hydrophobic tube," Phys. Fluids **29**, 062105 (2017).

[23] S. Yun, "Bouncing of an ellipsoidal drop on a superhydrophobic surface," Sci. Rep. **7**, 17699 (2017).

[24] A. Lafuma and D. Quéré, "Superhydrophobic states," Nat. mater. **2**, 457–460 (2003).

[25] A. Gauthier, S. Symon, C. Clanet, and D. Quéré, "Water impacting on superhydrophobic macrotextures," Nat. Commun. **6**, 8001 (2015).

[26] C. Clanet, C. Béguin, D. Richard, and D. Quéré, "Maximal deformation of an impacting drop," J. Fluid Mech. **517**, 199–208 (2004).